

## Mesoporous Carbons Prepared by Nano-Casting with Meso- or Non-Porous Silica Nanoparticles

Camila Ramos da Silva, Martin Wallau<sup>#</sup> and Ernesto A. Urquieta-González\*

Universidade Federal de São Carlos, Departamento de Engenharia Química CP 676,  
13565-905 São Carlos-SP, Brazil

Carbonos mesoporosos foram obtidos via nano-moldagem utilizando como molde: (i) nanoesferas de sílica mesoporosa com estrutura análoga à MCM-41 ou MCM-48; (ii) nanoesferas de sílica não-porosa e (iii) sílica pirogênica (Aerosil 200). Estes moldes de sílica (patrix) foram impregnados com sacarose e carbonizados em atmosfera de nitrogênio a 800 °C, sendo posteriormente a sílica dissolvida com ácido fluorídrico. Foi observado que a área superficial específica das matrizes de carbono pode ser aumentada diminuindo o diâmetro das nanoesferas de sílica ou a distância entre elas via aglomeração antes da impregnação do molde de sílica com a sacarose. Carbonos mesoporosos com áreas superficiais maiores que 500 m<sup>2</sup> g<sup>-1</sup> foram obtidos a partir de esferas de sílica mesoporosa. Neste caso, as matrizes de carbono contem mesoporos com estreita distribuição de tamanho e com diâmetros da ordem da espessura da parede da sílica mesoporosa utilizada como molde.

Mesoporous carbons were obtained by sequential nano-casting using the following hard templates: (i) mesoporous silica nanospheres with MCM-41 or MCM-48 analogous structure; (ii) non-porous silica nanospheres and (iii) pyrogenic silica (Aerosil 200). These silica templates (patrix) were impregnated with sucrose, carbonized at 800 °C under nitrogen atmosphere and finally the silica dissolved with hydrofluoric acid. It was observed that the specific surface area of the carbon matrixes can be enhanced reducing the diameter of the silica nanospheres or the distance between them by agglomeration prior to the impregnation of the silica patrix with sucrose. Mesoporous carbons with specific surface areas higher than 500 m<sup>2</sup>g<sup>-1</sup> were obtained using mesoporous silica spheres. In this case, the carbon matrixes contain mesopores with a narrow pore size distribution and with diameters in the order of the wall thickness of the mesoporous silica used as hard template.

**Keywords:** nano-casting, porous carbon, non-porous silica, mesoporous silica, MCM-41, MCM-48, nanospheres

### Introduction

Mesoporous carbons possessing ordered pore structures, high surface area and large pore volume are of great interest due to their potential applications such as catalysts, adsorbents and as carriers in the energy storage.<sup>1</sup> Considering their uniform pore structure and high surface area they are also widely studied as hard template (matrix)<sup>2</sup> for the crystallisation of mesoporous zeolites<sup>3</sup> or high surface metal oxides.<sup>4</sup> In the last years, the use of ordered mesoporous silicas as hard template

(patrix) for the preparation of ordered mesoporous carbon was widely studied.<sup>5,6</sup> The principle of this nano-casting technique for the preparation of ordered mesoporous carbons is illustrated in Figure 1. In a first step, the mesoporous silica “patrix” is filled with a carbon precursor either by impregnation with a carbon precursor such as sucrose,<sup>7</sup> followed by carbonisation or by chemical vapour deposition.<sup>8</sup> Once that the carbon

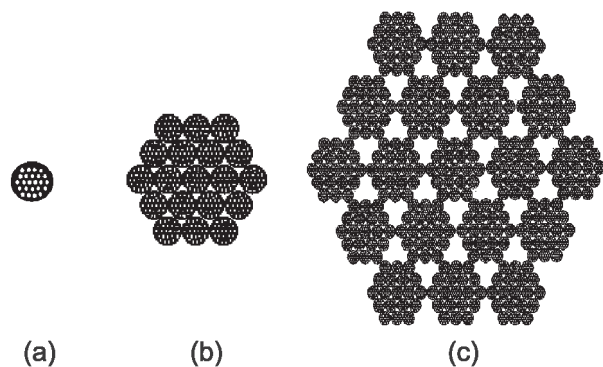


Figure 1. Preparation of mesoporous carbons by nano-casting.

\*e-mail: urquieta@power.ufscar.br

<sup>#</sup>Present Address: Universidade Federal de Pelotas, Instituto de Química e Geociências, CP 354, 96010-900 Pelotas – RS, Brazil

structure is formed in the pores of the silica structure, the silica can be removed by dissolution in hydrofluoric acid or in diluted alkali hydroxides solution resulting in a mesoporous carbon replica (“matrix”) of the silica patrix, where the pores correspond to the walls of the original silica structure and the carbon walls to the mesopores of the silica. To avoid the collapse of the carbon structure into unstructured skeins of carbon fibres after the silica dissolution, only silica structures with a three-dimensional interconnected pore system, such as SBA-15,<sup>9</sup> MCM-48<sup>10</sup> or agglomerated silica spheres<sup>11</sup> are suitable as hard templates. On the other hand, the use of agglomerated porous silica spheres opens the possibility to prepare hierarchically ordered pore systems<sup>12</sup> as it is schematically shown in Figure 2, allowing the preparation of multi level ordered porous materials possessing meso - and macropores, where the first level is originated from the ordered mesopores inside the primary spheres (Figure 2a), the second level is a result of the pores between the primary spheres in the agglomerate (Figure 2b) and a third level can be created by the voids between such agglomerates (Figure 2c). The pore diameter of all of these pore levels can be adjusted by the diameter of the agglomerates (3<sup>rd</sup> level), the primary spheres (2<sup>nd</sup> level) and the mesopore system (1<sup>st</sup> level). Until now, silica spheres with mesoporous systems analogous to MCM-41, MCM-48<sup>12</sup> or SBA-15<sup>13</sup> have been described. The first two structures possessing hexagonal and cubic mesopore arrangement, respectively,<sup>10</sup> are prepared combining the



**Figure 2.** Hierarchically ordered pore system by agglomeration of porous spheres.

hydrolysis of tetraethylorthosilicate (TEOS) in the presence of cetyltrimethylammonium cations and water, ethanol and ammonia (known as Stöber method<sup>14</sup> for the preparation of monodispersed silica spheres), while the SBA-15 analogous silica spheres are obtained by hydrolysis of TEOS in acid media in the presence of the amphiphilic triblock copolymer Pluronic P123.<sup>13</sup> It is known, that the Stöber method allows the variation of the mean sphere diameter within a wide range,<sup>11</sup> therefore, the adjusting of the mean sphere diameter will allow the variation of the interparticle voids, while the mesopore diameter can be influenced by the organic template used or by the addition of hydrophobic compounds into the reaction mixture.<sup>9,10</sup> Varying the pore structure of the silica patrix will further allow the tailoring of the textural properties of the final mesoporous carbon.

## Experimental

### Preparation of the silica patrices

Mesoporous silica spheres with hexagonal and cubic pore arrangement analogous to MCM-41 and MCM-48 were prepared at room temperature following the procedure developed by Lind *et al.*,<sup>12</sup> by dissolving cetyltrimethylammonium bromide (CTABr) in a mixture of water (H<sub>2</sub>O), ethanol (C<sub>2</sub>H<sub>5</sub>OH) and aqueous ammonia (NH<sub>3</sub>). This mixture was stirred for 10 min and subsequently tetraethyl orthosilicate (TEOS) was added and the stirring continued for 2 h. The mesoporous silica nanospheres were separated by filtration and dried at 60 °C. Nonporous silica spheres were prepared following the Stöber method<sup>14</sup> using slightly varied compositions.<sup>11,15</sup> A mixture of ammonia (25 wt%), water and ethanol was stirred for 15 min. After addition of the tetraethylorthosilicate (TEOS), the stirring was continued for additionally 15 min and subsequently the reaction was allowed to complete for 24 h. Due to the small sphere diameter, the separation of the silica spheres by filtration was not possible, so that the obtained suspensions of the nanospheres were submitted to the procedure described in the next section. The molar compositions used for the

**Table 1.** Molar composition used in the synthesis of silica patrices and the observed mean sphere diameter

Silica Patrix	Pore structure	TEOS/ mol	CTABr/ mol	NH <sub>3</sub> / mol	C <sub>2</sub> H <sub>5</sub> OH/ mol	H <sub>2</sub> O/ mol	Sphere diameter/ nm
P41	Hexagonal	1	0.3	11	58	144	900 – 1000
P48	Cubic	1	0.4	12.5	54	174	900 -1000
Pa	Non-porous	1	-	1.4	104	65	160
Pb	Non-porous	1	-	4	75	15	260

synthesis of the silica spheres and their observed mean diameters are summarised in Table 1. Also pyrogenic silica (Aerosil 200), which consists of primary silica particles with mean diameters of 12 nm<sup>16</sup> aggregated into larger spheres was used as patrix for the preparation of porous carbon.

#### Preparation of the carbon matrixes

The carbon matrixes were prepared following a slightly modified recipe published by Yu *et al.*<sup>17</sup> First, the suspensions of non-porous silica spheres (patrices Pa and Pb) and the mesoporous silica spheres with cubic pore structure (patrix P48), re-dispersed by ultra-sonification in water, were aggregated by centrifugation at 3000 rpm for 3 h. The supernatant liquid was carefully removed with a pipette and the aggregates dried at 120 °C for 72 h. Finally, the aggregates were sintered at 700 °C for 2 h (heating rate 50 °C min<sup>-1</sup>). Subsequently, these silica moulds were first soaked with an aqueous solution of sucrose (66 wt%) and sulphuric acid, in the proportion of 0.1 g H<sub>2</sub>SO<sub>4</sub> per 1 g of sucrose and then dried at 100 °C in air. The sucrose impregnated solid was subsequently carbonised in nitrogen atmosphere at 800 °C (heating rate of 1 °C min<sup>-1</sup>). The porous carbon was generated by dissolving the inorganic part of the silica/carbon composite with hydrofluoric acid. After extensive washing with distilled water, the carbon matrix was dried at 110 °C. The obtained carbon matrixes were denominated Ma, Mb and M48<sub>aggl</sub>.

Using powders of uncalcined mesoporous silica spheres with hexagonal and cubic pore structure (P41 and P48) or Aerosil 200 (P<sub>Aerosil</sub>) as patrix mesoporous carbons were prepared by mixing the respective patrix powders with the above described sucrose and H<sub>2</sub>SO<sub>4</sub> solution and then kneading this mixture with a spatula until a uniform mass was obtained. After drying in air overnight at room temperature and subsequently at 100 °C for 5 h (heating rate 1 °C min<sup>-1</sup>), the occluded surfactant molecules (in the case of P41 and P48) and the adsorbed sucrose were carbonised under nitrogen atmosphere at 800 °C for 5 h (heating rate 1 °C min<sup>-1</sup>). Finally the parent silica structure was removed by dissolution with hydrofluoric acid (40 weight%). The mesoporous carbon was washed with distilled water and dried at 100 °C. The obtained porous carbons matrixes were denominated as M41, M48 and M<sub>Aerosil</sub>. An amount of sucrose solution (66 wt% with 0.1 g H<sub>2</sub>SO<sub>4</sub> per 1 g sucrose) was also dried and carbonised under the same conditions but in the absence of any silica patrix. The resulting carbon matrix was denominated M<sub>uncast</sub>.

#### Characterisation

The N<sub>2</sub> sorption analyses of the silica patrices and the mesoporous carbon matrixes were carried out on a Quantachrome Corporation (Nova-1200) instrument. In the case of the mesoporous silica spheres they were priory calcined at 700 °C. Previous to the analysis, about 0.05 g of each sample were treated under vacuum at 150 °C for 2 hours. From the N<sub>2</sub> sorption data, the specific surface area was estimated by the BET equation.<sup>18</sup> The pore size distribution and the mesoporous analysis were done from the desorption branch of the isotherm using the Barrett-Joyner-Halenda (BJH) method,<sup>19</sup> while the micropore volume was estimated by the t-plot analysis from the adsorption branch of the isotherm.<sup>20</sup>

The silica patrices and the carbon matrixes were further characterised by Scanning Electron Microscopy. Prior to the analysis, the samples were dispersed in acetone in an ultrasound bath. The resulting dispersion was dropped on the sample holder and after evaporation of the acetone the holder was sputtered with gold.

The mesoporous silica spheres with pore systems analogous to MCM-41 and MCM-48 as well as the mesoporous carbons prepared by using them as patrix were also characterised in the small angle X-ray diffraction (SAXRD) using a Siemens D5000 powder diffractometer operated with a Cu-K $\alpha$  radiation (33 kW and 50 mA) in the range of  $0.6 \leq 2\theta \leq 10^\circ$  ( $2\theta$ ).

The FTIR spectra of the dried P<sub>Aerosil</sub>/sucrose mixture and the porous carbon M<sub>Aerosil</sub> were recorded using the KBr pellet technique on a Perkin Elmer (Spectrum 100) FTIR Spectrometer from 500 to 4000 cm<sup>-1</sup> with 32 scans and 4 cm<sup>-1</sup> resolution.

The dried P<sub>Aerosil</sub>/sucrose mixtures and the porous carbon matrix M<sub>Aerosil</sub> were further studied by thermogravimetry from 25 to 1000 °C (heating rate of 10 °C min<sup>-1</sup>) under air flow using approximately 10 mg of the respective solid on a Thermal Analyst 2100 (TA Instruments) thermobalance.

## Results

#### Silica patrices

Figure 3 shows the nitrogen isotherms of the mesoporous and of the agglomerated non-porous silica spheres used as patrices for the preparation of porous carbon. The specific surface area ( $S_{\text{BET}}$ ), the external specific surface area ( $S_{\text{ext}}$ ), the micropore surface area ( $S_{\text{micro}}$ ), the total specific pore volume ( $V_{\text{total}}$ ), the specific mesopore volume ( $V_{\text{meso}}$ ) and the specific micropore

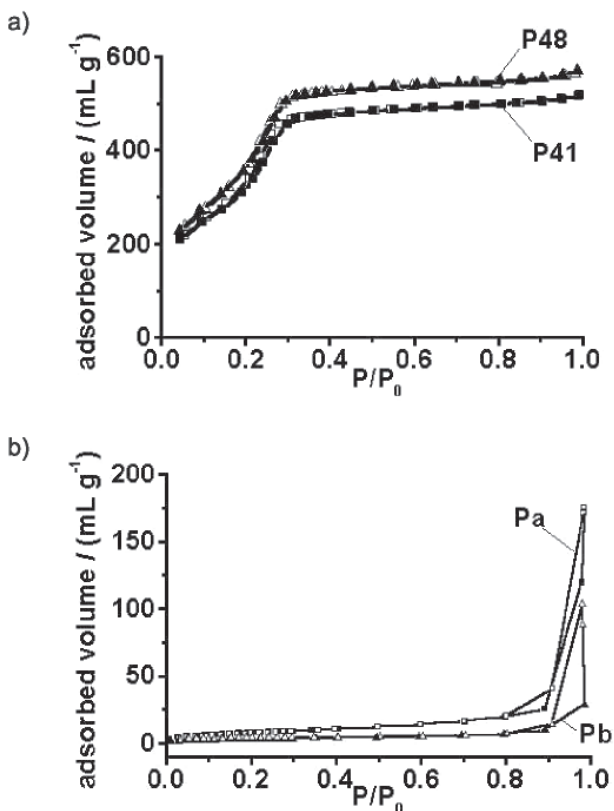


**Figure 3.** Nitrogen sorption isotherms of: (a) mesoporous silica patrices P41 and P48; (b) non-porous silica patrices Pa and Pb.

volume ( $V_{\text{micro}}$ ) observed for these silica patrices are summarised in Table 2, together with the mean pore radius of the patrices obtained from the maxima of the BJH pore size distributions shown in Figure 4. The textural properties reported for the pyrogenic silica<sup>16</sup> are also given in Table 2.

The isotherms of the mesoporous silica spheres P41 and P48 shown in Figure 3a can be classified by the IUPAC recommendations<sup>21</sup> as type IV, which are typical for ordered mesoporous materials. The sharp pore size distribution of the mesoporous silica spheres is confirmed by the BJH pore size distributions of P41 and P48 given in Figure 4a, which demonstrate that these samples possess very uniform mesopores with mean pore radius around 1.15 nm. Figure 4a further reveals the absence of

micropores in the calcined mesoporous silica spheres, as it is confirmed by the micropore volume of these samples reported in Table 2. The observed very high specific surface areas ( $S_{\text{BET}}$ ) of these samples (Table 2) are in the range reported for mesoporous silica spheres prepared at room temperature.<sup>12</sup>

The isotherms observed for the agglomerated non-porous silica spheres Pa and Pb, shown in Figure 3b, are according to the IUPAC recommendations<sup>21</sup> of type II, indicating non- or macro-porous adsorbents. It can be seen from Table 2 that these patrices have no microporosity and

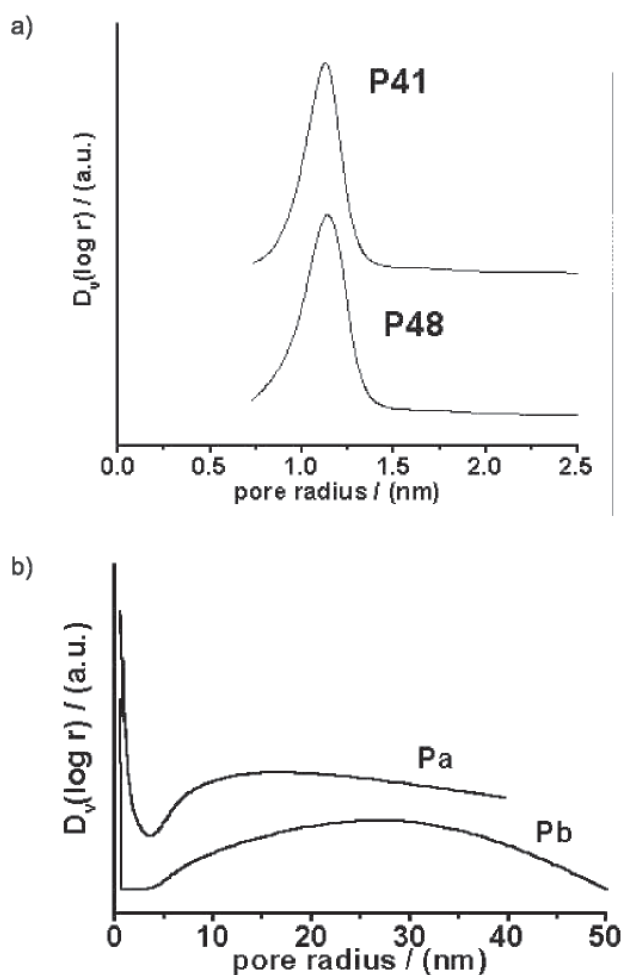


**Figure 4.** BJH pore size distribution of: (a) mesoporous silica patrices P41 and P48; (b) agglomerated non-porous silica patrices Pa and Pb.

**Table 2.** Textural properties of the used silica hard templates (patrices)

Silica Patrice	$S_{\text{BET}} / (\text{m}^2 \text{g}^{-1})$	$S_{\text{ext}} / (\text{m}^2 \text{g}^{-1})$	$S_{\text{micro}} / (\text{m}^2 \text{g}^{-1})$	$V_{\text{total}} / (\text{mL g}^{-1})$	$V_{\text{meso}} / (\text{mL g}^{-1})$	$V_{\text{micro}} / (\text{mL g}^{-1})$	$r_{\text{pore}} / \text{nm}$
P41	1267	1267	0	0.799	0.799	0	1.15
P48	1402	1402	0	0.870	0.870	0	1.15
Pa	26	26	0	0.271	0.271	0	> 10
Pb	15	15	0	0.137	0.137	0	18
P <sub>Aerosil</sub> *	200 ± 25	-	-	-	-	-	-

\*Reference 16.

very low specific surface area and pore volume as is expected for agglomerates of non-porous silica spheres. The observed specific surface area ( $S_{\text{BET}}$ ) reported in Table 2, of  $26 \text{ m}^2\text{g}^{-1}$  for sample Pa and  $15 \text{ m}^2\text{g}^{-1}$  for sample Pb corresponds roughly to the geometrical surface area ( $S_{\text{GEO}}$ ) of 21 and  $14.5 \text{ m}^2\text{g}^{-1}$  for amorphous silica spheres with 160 and 230 nm in diameter, respectively, calculated by the equation 1 considering a density of around  $1.8 \text{ g mL}^{-1}$ .<sup>22</sup> As can be seen from the pore size distributions of Pa and Pb given in Figure 4b, pore radii larger than 10 nm can be observed for sample Pa, which corresponds to the radii of interstices between 12 and 33 nm, which are expected for close-packed spheres with diameters around 160 nm. Also the pore radii around 28 nm observed for sample Pb (Figure 4b) are in the range of the pore radii expected for interstices between 20 to 34 nm, corresponding to close packed spheres with diameters around 230 nm.

$$S_{\text{GEO}} = \frac{S_{\text{sphere}}}{V_{\text{sphere}} \cdot \rho} = \frac{4\pi r^2}{\left(\frac{4}{3}\right)\pi r^3 \cdot \rho} = \frac{3}{r \cdot \rho} = \frac{6}{d_{\text{sphere}} \cdot \rho} \quad (1)$$

The SAXRD patterns of the mesoporous silica patrices P41 and P48 are shown in Figure 5. The pattern of P48 shows six well resolved peaks which can be indexed in the  $Ia3d$  space group as indicated in Figure 5. The cubic unit cell parameter  $a = 9.62 \text{ nm}$  was calculated from the slope of the function  $1/(d_{\text{hkl}})^2 = (h^2 + k^2 + l^2)/a^2$ , determined by linear regression. In contrast, the ill resolved pattern of P41 shows only one broad peak at around  $2.3^\circ(2\theta)$ , which consequently indicates an ill ordered pore system, as it is also observed for mesoporous materials of the MSU type.<sup>23</sup> Assuming a fairly hexagonal pore arrangement in P41, the observed plane distance of 4.01 nm corresponds to the hexagonal unit cell parameter  $a$  of 4.47 nm.

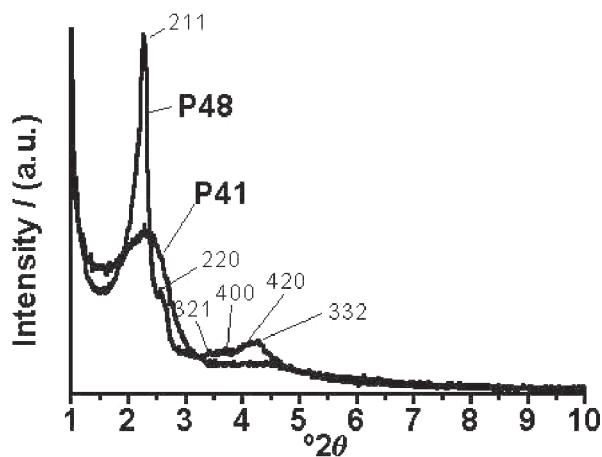


**Figure 5.** Small angle X-ray diffraction (SAXRD) patterns of mesoporous silica patrices P48 and P41.

The SEM micrographs of the applied silica patrices, including Aerosil 200 are demonstrated in Figure 6. The micrographs of the mesoporous silica spheres (Figure 6a and b) reveal that P41 and P48 consists of spheres with diameters around 900 to 1000 nm. The micrographs of the non-porous silica spheres, given in Figure 6c and 6d, show that very uniform spheres are obtained, whose mean diameters are 160 and 260 nm for sample Pa and Pb, respectively. For the pyrogenic silica Aerosil 200, the SEM micrograph (Figure 6e) shows the presence of spherical particles with mean diameters in the range of 10 nm. However, here one should consider the fact that such Aerosil particles are known to consist of primary particles for which diameters around 12 nm are reported.<sup>16</sup>

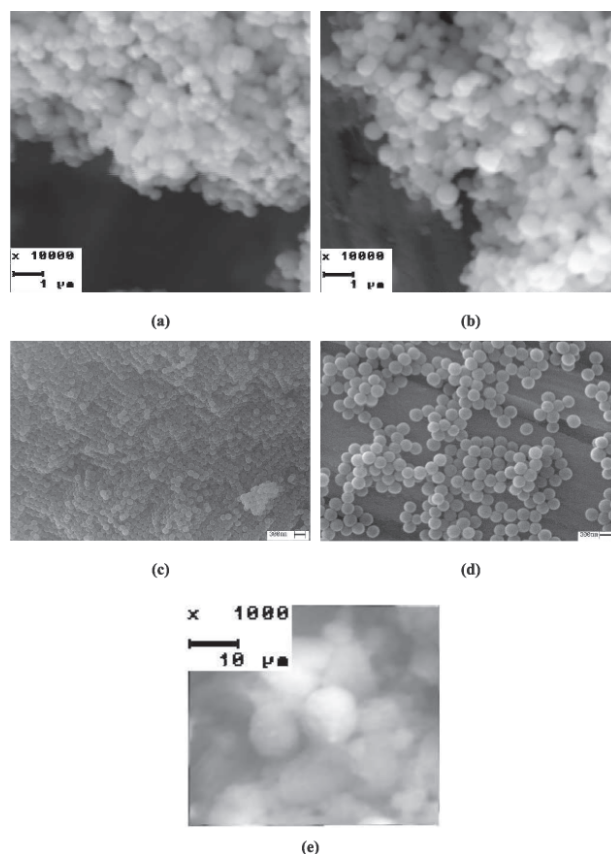


**Figure 6.** SEM micrographs of the used silica patrices: (a) P48; (b) P41; (c) Pa; (d) Pb; (e) Aerosil 200.

#### Carbon matrixes

Figure 7 shows the nitrogen isotherms of the porous carbon matrixes obtained by nano-casting from the different silica patrices described above and of the carbon obtained by carbonisation of the sucrose in the absence of any silica patrix. The specific surface area ( $S_{\text{BET}}$ ), the external specific surface area ( $S_{\text{ext}}$ ), the micropore surface area ( $S_{\text{micro}}$ ), the total specific pore volume ( $V_{\text{total}}$ ), the

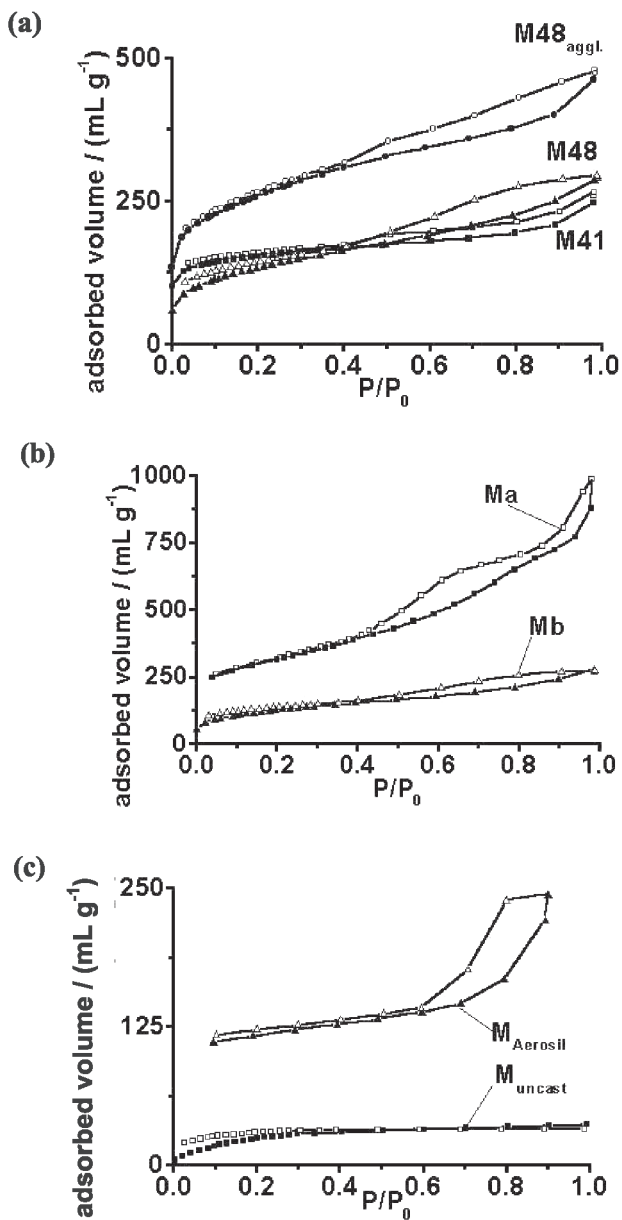


**Figure 7.** Nitrogen sorption isotherms of: (a) carbon matrixes M41, M48 and M48<sub>aggl.</sub>; (b) carbon matrixes Ma and Mb; (c) carbon matrixes M<sub>Aerosil</sub> and M<sub>uncanst</sub>.

specific mesopore volume ( $V_{\text{meso}}$ ) and the specific micropore volume ( $V_{\text{micro}}$ ) observed for these carbons are summarised in Table 3 together with their mean pore radius taken from the maximum of their BJH pore size distributions shown in Figure 8.

For M48 the surface area and pore volume given in Table 3 are much lower than the surface area and the pore volume reported for CMK-1, a mesoporous carbon prepared by nano-casting with MCM-48 as patrix, for which a specific surface area of  $1380 \text{ m}^2 \text{ g}^{-1}$  and a specific pore volume of  $1.4 \text{ mL g}^{-1}$  are observed.<sup>5</sup> It can be seen from the values given in Table 3 and from the nitrogen

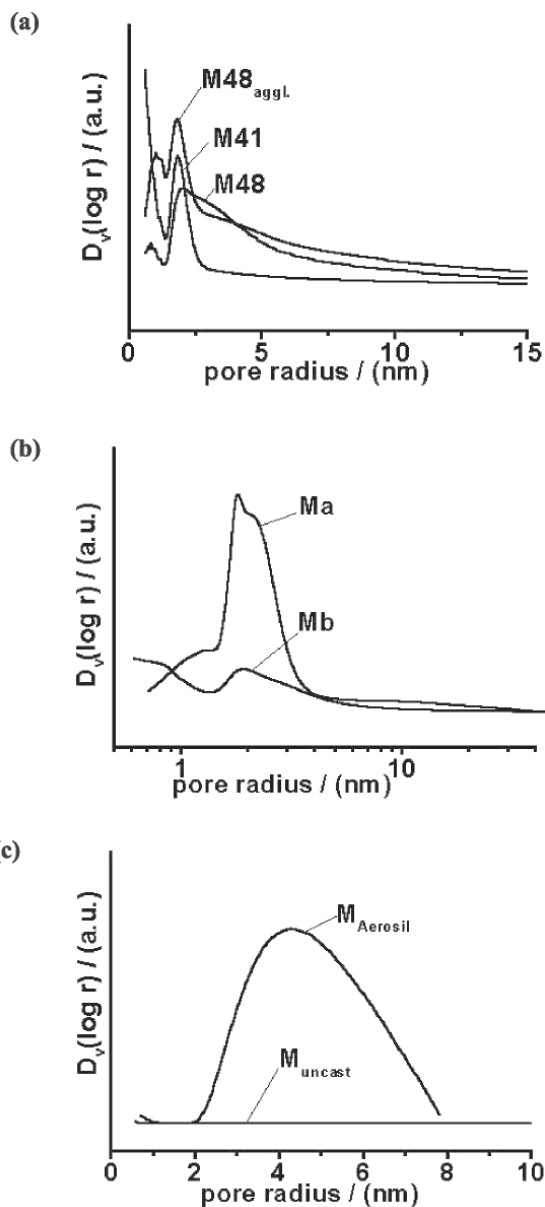


**Figure 8.** BJH pore size distribution of: (a) carbon matrixes M41, M48 and M48<sub>aggl.</sub>; (b) carbon matrixes Ma and Mb; (c) carbon matrixes M<sub>Aerosil</sub> and M<sub>uncanst</sub>.

isotherm and the BJH pore size distribution shown in Figure 7c and Figure 8c, respectively, that for the M<sub>uncanst</sub> matrix a carbon with low surface area and without any micro- and meso-porosity was formed when sucrose was carbonised in the absence of a silica patrix. This result could explain the relative low surface area and pore volume observed for M48, where the formation of non-porous carbon could have occurred during the carbonisation of sucrose deposited in the interstices between the MCM-48 spheres.

Another difference between CMK-1<sup>5</sup> and M48 is the broader pore size distribution observed for M48. While

CMK-1 shows a sharp mesopore size distribution with a mean pore radius of 1.5 nm, M48 shows broad bimodal mesopore size distribution. As it can be seen from Figure 8, M48 shows a relatively sharp distribution of mesopores with a mean radius of 1.82 nm and a second type of mesopores with a broad size distribution with a maximum around 3.12 nm. As M48 was prepared mixing uncalcined silica P48 with the sucrose solution, the content of organic material present in the P48 mesopores might have been lower during the preparation of M48 than during the preparation of CMK 1. Thus, the incomplete filling of the pores of the P48 patrx might have resulted in the formation of irregular mesopores. The formation of irregular mesopores due to the incomplete filling of the P48 mesopores is strengthened by the pore size distribution of M48<sub>aggl.</sub> Prior to the preparation of the M48<sub>aggl.</sub> matrix the silica P48 spheres were calcined and the complete filling of the mesopores with the sucrose solution was confirmed by the transparency of the sucrose impregnated P48 patrx. As it can be seen from Figure 8a, the carbon M48<sub>aggl.</sub> shows a very regular bimodal mesopore size distribution with mean radii at around 1.0 and 1.8 nm. The surface area and the pore volume of M48<sub>aggl.</sub> are also much higher than that of M48.

On the other hand, the nitrogen isotherm and the BJH pore size distribution of M41, as well as their textural properties given in Table 3, unexpectedly reveal that a mesoporous carbon with regular mesopores is formed when mesoporous silica spheres with a pore structure analogous to MCM-41 are used as patrx. It was found by Kruk *et al.*<sup>24</sup> that carbonisation in the one-dimensional pores of MCM-41 results in the formation of high-surface-area disordered microporous carbon. Therefore, the presence of regular mesopores in M41 indicates that the silica P41 possesses a system of interconnected mesopores, as it is known for SBA-15 and MSU type mesoporous silica, which possess hexagonally arranged mesopores interconnected by micropores.<sup>25,26</sup> As micropores were not detected for P41, the presence of regular mesopores in M41 suggests a system of interconnected mesopores in the silica patrx P41. Although uncalcined P41, which

might still contain micropores, was used for the preparation of M41, the presence of interconnected mesopores in silica spheres analogous to MCM-41 could be confirmed using calcined silica spheres as patrx. As it is reported elsewhere,<sup>27,28</sup> the use of calcined silica spheres analogous to MCM-41 also results in mesoporous carbon with uniform mesopores showing a mean diameter around 2 nm. Furthermore, it was observed that that carbon presented higher specific surface area than M41, thus confirming that the use of uncalcined mesoporous silica results in poor pore filling and consequently in mesoporous carbon with a lower specific surface area.

As M41 is an inverse replica of the silica P41, the pore diameter in M41 should be equal to the wall thickness of P41. From the unit cell parameter and the mean pore radius of P41, its wall thickness can be estimated to 2.17 nm. This is approximately 3/5 of the pore diameter in M41, which is 3.68 nm. Such an increase in the pore diameter of the porous carbon, in comparison with the wall thickness of the used patrx, was attributed by Ryoo *et al.*<sup>5</sup> to a volume contraction during the pyrolysis of the organic compound infiltrated into the silica mesopores.

The corresponding carbon matrix Ma prepared from the silica patrx Pa shows a high specific surface area (1124 m<sup>2</sup> g<sup>-1</sup>) and as it can be seen from Figure 8b, a large mesopore distribution with maximum at around 1.8 nm. These mesoporous system might correspond to windows connecting the cavities generated by the dissolution of the silica nanospheres. The carbon matrix Mb prepared from the silica patrx Pb, whose spheres possess a larger mean diameter than the spheres of the silica patrx Ma, shows a smaller specific surface area and pore volume than the carbon matrix Ma (Table 3). As it can be seen from Figure 8b, also a much broader pore size distribution is observed for the matrix Mb.

As it can be seen from Figure 8c, the use of Aerosil 200 as patrx leads to a mesoporous carbon M<sub>Aerosil</sub> with a very broad pore size distribution. It should be remarked that the carbon matrix M<sub>Aerosil</sub> contains a relatively large amount of micro- and mesopores as it is revealed by their specific pore volumes  $V_{meso}$  (0.241 mL g<sup>-1</sup>) and  $V_{micro}$  (0.147

**Table 3.** Textural properties of the prepared carbon matrixes

Carbon Matrix	$S_{BET}/(m^2 g^{-1})$	$S_{ext}/(m^2 g^{-1})$	$S_{micro}/(m^2 g^{-1})$	$V_{total}/(mL g^{-1})$	$V_{meso}/(mL g^{-1})$	$V_{micro}/(mL g^{-1})$	$r_{pore}/nm$
M41	589	262	327	0.410	0.260	0.135	1.8
M48	534	429	105	0.459	0.399	0.047	0.9/1.8/3.1
M48 <sub>aggl.</sub>	856	851	5.4	0.714	0.674	0.040	1.1/1.8
Ma	1124	852	272	1.524	1.413	0.121	2.7/10.5
Mb	487	387	100	0.424	0.369	0.045	1.5-10.0
M <sub>Aerosil</sub>	369	148	220	0.376	0.241	0.147	4.5
M <sub>uncast</sub>	61	61	0	0.056	-	-	-

mL g<sup>-1</sup>) reported in Table 3. As it can be seen from the isotherms (Figure 7c), the BJH pore size distribution (Figure 8c) and the textural properties reported in Table 3, a non-porous carbon (M<sub>un-*cast*</sub>) is obtained when the sucrose solution is dried and carbonised in the absence of any silica patrix.

The small angle XRD patterns of porous carbon matrixes M41 and M48 (Figure 9) show very broad peaks. The peak at around 2.5 °(2θ) observed for M48 can be attributed to the reflection of *d*<sub>211</sub> planes and the broad one at 4.7 °(2θ) to the overlapped reflections of the *d*<sub>430</sub> and *d*<sub>332</sub> planes corresponding to the cubic *Ia3d* symmetry. From the *d*<sub>211</sub> reflection, a unit cell parameter “*a*” of 8.65 nm can be estimated. The °(2θ) values of the *d*<sub>430</sub> and *d*<sub>332</sub> plane reflections expected for such unit cell parameter are 4.6 and 4.8 °(2θ), respectively, which coincidences with the maximum of 4.7 °(2θ) observed in the XRD pattern of M48. The maximum of the peak observed in the pattern of M41 is around 2.2 °(2θ), which can be attributed to a hexagonal unit cell parameter “*a*” of 4.63 nm.

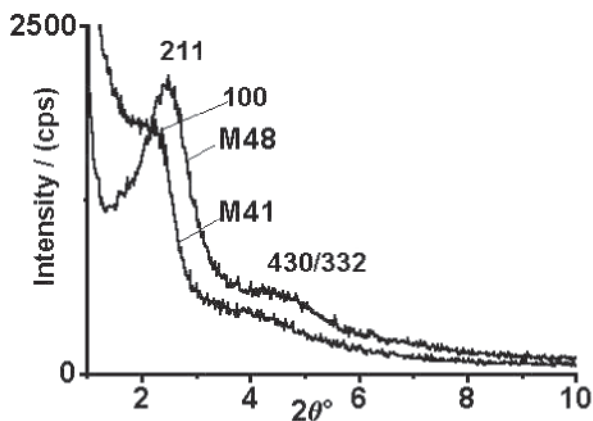


**Figure 9.** Small angle X-ray diffraction (SAXRD) patterns of mesoporous carbon matrixes M48 and M41.

Figure 10 shows the SEM micrographs of the porous carbon matrixes. It can be seen from Figure 10a that M41 appears as an aggregation of plate-like carbon particles with spherical holes in the range of 1000 nm, which indicates the imprinting of the P41 nanospheres in the obtained carbon. As the P41 mould and the sucrose were mixed here by simple kneading of the nanospheres wetted with the sucrose solution, the arrangement of these macropores is completely irregular. Furthermore, the macropores are separated by relative large areas of carbon, which was formed without any imprinting. The presence of a large number of holes in M41, which correspond to the P41 spheres further indicates that no or only a less extended interconnected carbon framework was formed by the

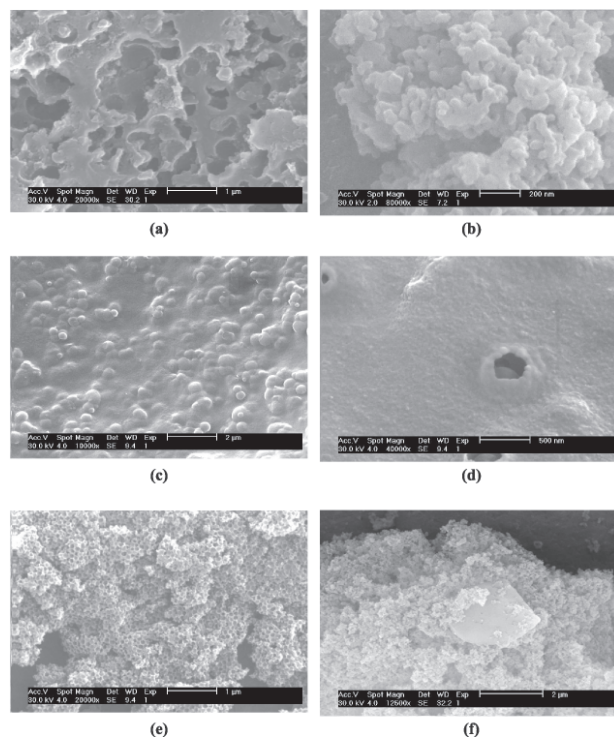


**Figure 10.** SEM micrographs of the carbon matrixes: (a) M41; (b) M48; (c) M48<sub>aggl.</sub>; (d) detail of M48<sub>aggl.</sub>; (e) Ma; (f) Mb.

carbonisation of uncalcined MCM-41 spheres impregnated with sucrose.

For the carbon matrix M48 (Figure 10b) also aggregated plate-like carbon particles showing imprinted holes are observed. However, the size and number of these holes is lower than in M41, thus suggesting that at least part of the surfactant molecules carbonised in the MCM-48 were incorporated into the formed carbon structure. Nevertheless, even M48 contains large areas of non-porous carbon, resulting in a low specific surface area.

When agglomerated and calcined MCM-48 were used as hard template the resulting carbon matrix (M48<sub>aggl.</sub>) appears as irregular agglomerate of carbon spheres probably due to the irregular shapes of the silica sphere matrixes. Although the carbon spheres observed in Figure 10c are seemingly compact, it is possible that they are partially hollow, as can be observed in Figure 10d, thus indicating that the carbon was formed mainly at the surface of the MCM-48 spheres.

The SEM micrographs of the carbon matrixes Ma and Mb shown in Figures 10e and 10f indicate the presence of irregular macropores, whose diameters are higher than that of the spheres used as patrix, indicating contraction of the organic material during the carbonisation. However, for Mb (Figure 10f) also nonporous carbon, probably formed by carbonisation of sucrose deposited at the surface of the agglomerated silica spheres can be observed.

The FTIR spectra of the dried  $P_{\text{Aerosil}}$ /sucrose composite and the resulting carbon matrix  $M_{\text{Aerosil}}$ , given in Figure 11, shows for the first<sup>29</sup> the presence of C-OH groups (bands at around 3423, 1641, 1381 and 1073  $\text{cm}^{-1}$ ), C=O groups (band at 1737  $\text{cm}^{-1}$ ) and  $\text{CH}_2$  and  $\text{CH}_3$  groups (bands at 2936 and 2359  $\text{cm}^{-1}$ ) indicating that the impregnated sucrose is still present after drying of the composite. After carbonisation and silica dissolution these bands attributed to the impregnated sucrose molecules are strongly decreased, which indicates the nearly complete decomposition of the organic material. On the other hand, bands at around 1384 and 1596  $\text{cm}^{-1}$ , which would indicate the formation of graphite like structures<sup>30,31</sup> cannot be observed in the  $M_{\text{Aerosil}}$  matrix.

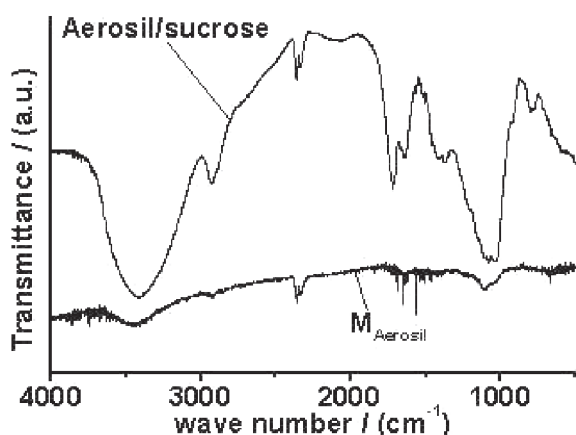


**Figure 11.** FTIR spectra of the dried  $P_{\text{Aerosil}}$ /sucrose composite and of the carbon matrix  $M_{\text{Aerosil}}$ .

The thermogravimetric analysis (TGA) and differential thermogravimetric analysis (DTG) of the dried  $P_{\text{Aerosil}}$ /sucrose composite and the resulting carbon matrix  $M_{\text{Aerosil}}$  are shown in Figure 12. It can be seen that for the  $P_{\text{Aerosil}}$ /sucrose composite (Figure 12a) the occluded material is burned off in three steps around 176, 344 and 542  $^{\circ}\text{C}$ . These different steps indicate that the occluded sucrose forms various intermediates during its decomposition. It can be further seen from Figure 12a that after 600  $^{\circ}\text{C}$ , when 90% of the sample mass is already burned off, no further mass loss can be observed up to 1000  $^{\circ}\text{C}$ . On the contrary, for the carbon matrix  $M_{\text{Aerosil}}$  the occluded material is burned off in two steps around 68 and 638  $^{\circ}\text{C}$  (Figure 12b). These two steps can be attributed to the desorption of water physically adsorbed on the carbon matrix and the decomposition of the formed carbon structure which occurs, in contrast to the decomposition of the sucrose, without the formation of intermediates. For the decomposition of the carbon matrix  $M_{\text{Aerosil}}$  a mass loss of 100% is observed after 690  $^{\circ}\text{C}$  (Figure 12b). The fact that the carbon matrix is completely burned off shows

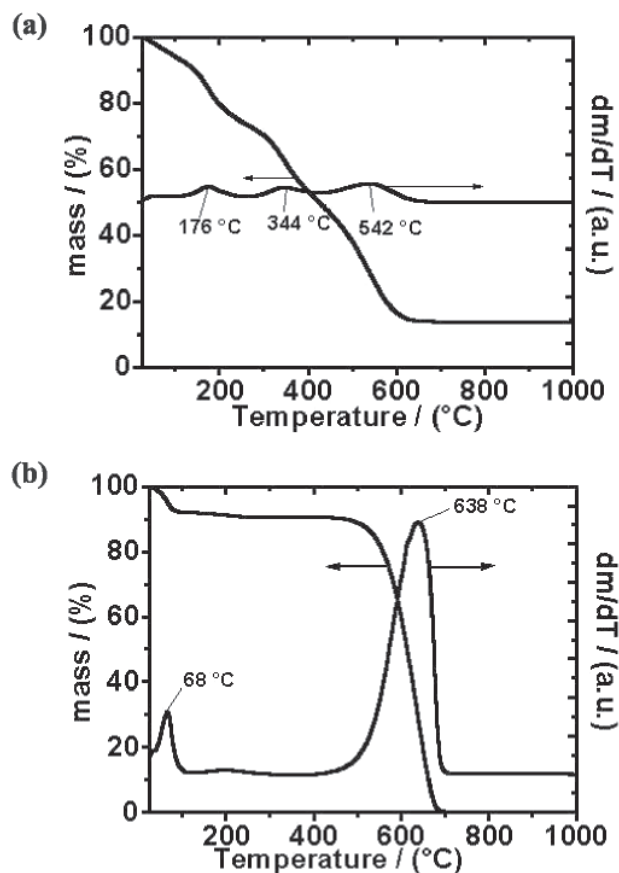


**Figure 12.** Thermogravimetry of: (a) dried  $P_{\text{Aerosil}}$ /sucrose composite; (b) carbon matrix  $M_{\text{Aerosil}}$ .

that dissolution in hydrofluoric acid at room temperature overnight is sufficient for the complete removal of the silica matrix.

## Discussion

The obtained results indicate that the specific surface area and the pore size distribution of the carbon matrices prepared by nano-casting with different silica spheres as matrix are influenced by different factors. On one hand, when agglomerated silica spheres were used as matrix, porous carbon matrices with very high specific surface area and a relatively narrow pore size distribution are obtained as it can be seen in Table 3 and from the respective BJH pore size distribution shown in Figure 8a and 8b. Due to the similar refractive index of the silica and the solution of the concentrated sucrose, the agglomerates turned transparent when the pores of the agglomerates were filled with the sucrose solution, which permits to monitor the complete pore filling. After the filling of the pores, the imbibed agglomerates were further washed with alcohol to remove sucrose from the surface. When the sucrose was only mixed with the silica

powder, an opaque paste was obtained and the specific surface area of the carbon matrix is substantially smaller than that obtained using an agglomerate as patrix. As an example it can be seen in Table 3 that the specific surface area for M48 is 534 and for M48<sub>aggl</sub> 856 m<sup>2</sup> g<sup>-1</sup>. The reduced surface area of the matrix obtained by simple mixing the patrix with the sucrose solution is probably due to the formation of non-porous carbon during the carbonisation of sucrose, which is formed without the influence of the silica patrix. This fact is supported by the small surface area of M<sub>uncast</sub> (61 m<sup>2</sup> g<sup>-1</sup>) and the pore size distribution (Figure 8c) of the non-porous carbon obtained when the sucrose is carbonised in the absence of a silica patrix. Therefore, the carbonisation of sucrose which is not in close contact with the silica patrix will result in the formation of non porous carbon, thus reducing the specific surface area of the formed carbon. However, even for carbon matrixes prepared from agglomerated spheres, incomplete pore filling (see SEM micrograph of M48<sub>aggl</sub> in Figure 10d) or formation of non-porous carbon at the surface of the agglomerates of spheres (see SEM micrograph of sample Mb in Figure 10f) was observed.

On the other hand, the specific surface area is strongly influenced by the radius of the patrix spheres. This can be clearly observed from Table 3, where the carbon matrix Ma with nanosphere diameter of 160 nm has a specific surface area of 1124 against 487 m<sup>2</sup> g<sup>-1</sup> of the carbon matrix Mb, whose nanosphere diameter is 260 nm. Nevertheless, one would expect for M<sub>Aerosil</sub>, which was prepared using primary silica particles with diameters around 12 nm,<sup>16</sup> a very high specific surface area. However, the observed specific surface area of such M<sub>Aerosil</sub> is only 369 m<sup>2</sup>g<sup>-1</sup> (Table 3). As this matrix was prepared by mixing the sucrose solution with the Aerosil powder, that relatively low area is probably due to the formation of large amounts of non-porous carbon. As it can be seen from Figure 12a, the P<sub>Aerosil</sub>/sucrose composite contains 90% of organic material, thus indicating that large parts of the sucrose were not in close contact with the silica patrix.

The obtained results clearly indicate that using mesoporous silica spheres analogous to MCM-41 and MCM-48 as patrix, mesoporous carbon matrixes M41, M48 and M48<sub>aggl</sub> with a relatively narrow pore size distribution are obtained (Figure 8a), where mesopores around 2 nm, which roughly corresponds to the wall thickness of the used silica patrix, are observed. Mesoporous carbon with uniform pore diameters is also obtained when calcined MCM-41 analogous silica spheres are used as cast,<sup>27,28</sup> thus indicating that these spheres possess a interconnected system of mesopores.

The presence of interconnected mesopores in these MCM-41 analogous silica confirms their building mechanism proposed by Tan *et al.*<sup>32</sup> These authors suggested as a first step in the formation of mesoporous silica spheres a nucleation of disordered silica/surfactant clusters. During the formation of the mesoporous silica spheres such clusters will form spherical aggregates less than 100 nm. Only during the growing of these aggregates occurs the alignment of the silica/surfactant micelles relative to the sphere surface, which may result in a hexagonal or cubic pore array. In the core of the mesoporous silica spheres, whose SAXRD indicated a hexagonal pore array analogous to MCM-41, Tan and Rankin<sup>32</sup> observed by transmission electron microscopy, besides zones with hexagonal pore array analogous to MCM-41, zones with cubic pore arrangement analogous to MCM-48 and zones with disordered pore arrangement. Such small zones with cubic or disordered pores contain partially interconnected mesopores and their replication in the carbon structure will stabilise the pore system after silica removal, thus explaining the presence of uniform mesopores in M41.

As it can be seen from the FTIR spectra of M<sub>Aerosil</sub>, given in Figure 11, the carbonisation process applied here reduces the CH<sub>2</sub>, CH<sub>3</sub> and COH units in the organic matrix but did not lead to the formation of graphite like structure units, so that the obtained carbon matrixes consist of amorphous carbon.

## Conclusions

Mesoporous carbon can be prepared by carbonisation of sucrose in the presence of silica nanospheres. The specific surface area of the carbon matrixes can be enhanced reducing the diameter of the silica nanospheres or reducing the distance between the silica nanospheres by agglomeration prior to the addition of the sucrose solution to the silica patrix. Mesoporous carbons with specific surface areas higher than 500 m<sup>2</sup> g<sup>-1</sup> are obtained using mesoporous silica spheres as patrix. In this latter case, the carbon matrixes contain mesopores with a narrow pore size distribution, where the pore diameters are in the order of the wall thickness of the mesoporous silica used as patrix.

## Acknowledgments

The authors gratefully acknowledge the financial support provided by CNPq/Brazil (grant 477759/2003-3 and 505157/2004-7). M. W. gives also acknowledgements to PVE-Program/Capes, Brazil.

## References

1. Lee, J. S.; Joo, S. H.; Ryoo, R.; *J. Am. Chem. Soc.* **2002**, *124*, 1156.
2. Stein, A.; *Microporous Mesoporous Mater.* **2001**, *44-45*, 227.
3. Schmidt, I.; Madsen, C.; Jacobson, C. J. H.; *Inorg. Chem.* **2000**, *39*, 2279.
4. Schwickardi, M.; Johann, T.; Schmidt, W.; Schüth, F.; *Chem. Mater.* **2002**, *14*, 3913.
5. Ryoo, R.; Joo, S. H.; Jun, S.; *J. Phys. Chem. B* **1999**, *103*, 7745.
6. Ryoo, R.; Joo, S. H.; Kruk, M.; Jaroniec, M.; *Adv. Mater.* **2001**, *13*, 677; Kaneda, M.; Tsubakiyama, T.; Carlsson, A.; Sakamoto, Y.; Ohsuna, T.; Terasaki, O.; Joo, S. H.; Ryoo, R.; *J. Phys. Chem. B* **2002**, *106*, 1256; Ryoo, R.; Joo, S. H.; Jun, S.; Tsubakiyama, T.; Terasaki, O.; *Studies in Surface Science and Catalysis* **2001**, *135*, 150; Jun, S.; Joo, S. H.; Ryoo, R.; Kruk, M.; Jaroniec, M.; Liu, Z.; Ohsuna, T.; Terasaki, O.; *J. Am. Chem. Soc.* **2000**, *122*, 10712; Joo, S. H.; Choi, S. J.; Oh, I.; Kwak, J.; Liu, Z.; Terasaki, O.; Ryoo, R.; *Nature* **2001**, *412*, 169; Lee, J.; Yoon, S.; Hyeon, T.; Oh, S. M.; Kim, K. B.; *Chem. Commun.* **1999**, 2177; Yoon, S. B.; Kim, J. Y.; Yu, J. S.; *Chem. Commun.* **2001**, 559; Yoon, S. B.; Kim, J. Y.; Yu, J. S.; *Chem. Commun.* **2002**, 1536; Lee, J.; Yoon, S.; Oh, S. M.; Shin, C. H.; Hyeon, T.; *Adv. Mater.* **2000**, *12*, 359; Kim, S. S.; Pinnavaia, T. J.; *Chem. Commun.* **2001**, 2418; Lee, J.; Kim, J.; Hyeon, T.; *Chem. Commun.* **2003**, 1138; Lee, J.; Sohn, K.; Hyeon, T.; *J. Am. Chem. Soc.* **2001**, *123*, 5146; Lee, J.; Sohn, K.; Hyeon, T.; *Chem. Commun.* **2002**, 2674; Yang, H.; Shi, Q.; Liu, X.; Xie, S.; Jiang, D.; Zhang, F.; Yu, C.; Zhao, D.; *Chem. Commun.* **2002**, 2842; Fan, J.; Yu, C.; Gao, F.; Lei, J.; Tian, B.; Wang, L.; Luo, B.; Tu, B.; Zhou, W.; Zhao, W.; *Angew. Chem., Int. Ed.* **2003**, *42*, 3146.
7. Wallau, M.; Dimitrov, L.; Urquieta-González, E. A.; *Studies in Surface Science and Catalysis* **2005**, *156*, 535.
8. Xia, Y.; Yang, Z.; Mokaya, R.; *Studies in Surface Science and Catalysis* **2005**, *156*, 565.
9. Zhao, D. Y.; Feng, J. L.; Huo, Q. S.; Fredrickson, G. H.; Chmelka, B. F.; Stucky, G. D.; *Science* **1998**, *279*, 548.
10. Beck, J. S.; Vartuli, J. C.; Roth, W. J.; Leonowicz, M. E.; Kresge, C. T.; Schmitt, K. D.; Chu, C. T. -W.; Olson, D. H.; Sheppard, E. W.; McCullen, S. B.; Higgins, J. B.; Schlenker, J. L.; *J. Am. Chem. Soc.* **1992**, *114*, 10834.
11. Ferreira, Y. K.; Wallau, M.; Urquieta-González, E. A.; *Studies in Surface Science and Catalysis* **2003**, *146*, 197.
12. Lind, A.; du Fresne v. Hohenesche, C.; Smått, J.-H.; Lindén, M.; Unger, K. K.; *Microporous Mesoporous Mater.* **2003**, *66*, 219.
13. Zhao, D.; Li, Q.; Stucky, G. D.; *Chem. Mater.* **2000**, *12*, 275.
14. Stöber, W.; Fink, A.; Bohn, E.; *J. Colloid Interface Sci.* **1968**, *26*, 62.
15. Giesche, H.; *J. Eur. Ceram. Soc.* **1994**, *14*, 189.
16. Anonymous, *Aerosil - Pyrogene Kieselsäuren*, Degussa AG: Hanau, without year.
17. Yu, J.-S.; Yoon, S. B.; Chai, G. S.; *Carbon* **2001**, *39*, 1442.
18. Brunauer, S.; Emmet, P. H.; Teller, E.; *J. Am. Chem. Soc.* **1938**, *60*, 1553.
19. Barret, E. P.; Joyner, L. G.; Halenda, P. P.; *J. Am. Chem. Soc.* **1951**, *73*, 373.
20. Lippens, B. C.; Linsen, B. G.; de Boer, J. H.; *J. Catal.* **1964**, *3*, 32.
21. Sing, K. S. W.; Everett, D. H.; Haul, R. A.; Moscow, L.; Pierotti, R. A.; Rouquerol, J.; Siemiewska, T.; *Pure Appl. Chem.* **1985**, *57*, 603.
22. Ferreira, Y. K.; *MSc. Dissertation*, Universidade Federal de São Carlos, Brazil, 2004.
23. Prouzet, E.; Cot, F.; Nabias, G.; Larbot, A.; Kooyman, P.; Pinnavaia, T. J.; *Chem. Mater.* **1999**, *11*, 1498.
24. Kruk, M.; Jaroniec, M.; Ryoo, R.; Joo, S. H.; *J. Phys. Chem. B* **2000**, *104*, 7960.
25. Bennadja, Y.; Beaunier, P.; Margolese, D.; Davidson, A.; *Microporous Mesoporous Mater.* **2001**, *44-45*, 147.
26. Joo, S. H.; Ryoo, R.; Kruk, M.; Jaroniec, M.; *J. Phys. Chem. B* **2002**, *106*, 4640.
27. Wallau, M.; Dimitrov, L. D.; Da Silva, C. R.; Urquieta-González, E. A.; *Studies in Surface Science and Catalysis*, **2006**, *162*, 409.
28. Wallau, M.; Dimitrov, L. D.; Da Silva, C. R.; Urquieta-González, E. A.; *Catal. Today*, submitted.
29. Hesse, M.; Meier, H.; Zeeh, B.; *Spektroskopische Methoden in der Organischen Chemie*, Thieme: Stuttgart, 1979.
30. Johnson, A.; Brigham, E. S.; Ollivier, P. J.; Mallouk, T. E.; *Chem. Mater.* **1997**, *9*, 2448.
31. Li, W. C.; Lu, A. H.; Guo, S. C.; *Carbon* **2001**, *39*, 1989.
32. Tan, B.; Rankin, S. E.; *J. Phys. Chem B* **2004**, *108*, 20122.

Received: March 12, 2006

Published on the web: October 3, 2006

FAPESP helped in meeting the publication costs of this article.